Pharm Res (2015) 32:2995–3006
DOI 10.1007/s11095-015-1681-7

RESEARCH PAPER

Focused Ultrasound as a Scalable and Contact-Free Method to Manufacture Protein-Loaded PLGA Nanoparticles

Stefan Schiller[1,2] • Andrea Hanefeld[2] • Marc Schneider[1] • Claus-Michael Lehr[1,3]

Received: 19 December 2014 / Accepted: 18 March 2015 / Published online: 31 March 2015

ABSTRACT

Purpose Although nanomaterials are under investigation for a very broad range of medical applications, only a small fraction of these are already commercialized or in clinical development. A major challenge for the translation of nanomedicines into the clinic is the missing scalability of the available lab scale preparation methods and, ultimately, non-identical samples during early and late research.

Methods Protein-loaded PLGA nanoparticles using focused ultrasound in an emulsion solvent diffusion method were prepared in different batch sizes to evaluate achievable mean size, protein loading, and yield.

Results Using the same equipment, nanoparticles could be prepared in batch sizes from 1 mg to 2.5 g. Size and yield were directly controllable by the amount of incident energy with good reproducibility. The nanoparticles displayed similar mean size, protein loading, and nanoparticle yield in batch sizes over three orders of magnitude. A scalable purification method based on diafiltration was established.

Conclusions The proposed method enables for feasibility studies during early research using just a small amount of polymer and protein, while at the same time it allows for larger scale production at later stages. As the proposed method further relies on contact-free energy transmission, it is especially suited for the preparation of clinical research samples.

KEY WORDS drug delivery · focused ultrasound · nanoparticles · nanotechnology · protein

ABBREVIATIONS

AIP	Average incident power
CR	Concentration reduction
DLS	Dynamic light scattering
DV	Diafiltration volumes
E	Total incident energy
EE	Encapsulation efficiency
EtOAc	Ethyl acetate
P-407 / P-188	Poloxamer 407 / 188
PIP	Peak incident power
PLGA	Poly(lactic-co-glycolic acid)
POE	Poly(oxyethylene)
POP	Poly(oxypropylene)
Y	Yield
T	Membrane transmission coefficient

INTRODUCTION

Nanomaterials are used in medicine in a variety of applications such as drug delivery, medical imaging, *in vitro* and *in vivo* diagnostics as well as tissue engineering (1). By encapsulating one or more drugs in nanoscale carrier systems with

Electronic supplementary material The online version of this article (doi:10.1007/s11095-015-1681-7) contains supplementary material, which is available to authorized users.

✉ Stefan Schiller
stefan.schiller@external.merckgroup.com

✉ Claus-Michael Lehr
claus-michael.lehr@helmholtz-hzi.de

[1] Department of Pharmacy, Biopharmaceutics & Pharmaceutical Technology, Saarland University, Campus, Building A4.1, 66123 Saarbrücken, Germany

[2] Research Pharmaceutics & Drug Product Development, Merck Serono, HPC D039/002, Frankfurter Str. 250, 64293 Darmstadt, Germany

[3] Department of Drug Delivery (DDEL), Helmholtz Institute for Pharmaceutical Research Saarland (HIPS), Helmholtz Center for Infection Research (HZI), Saarland University Campus, Building A4.1 66123 Saarbrücken, Germany

specifically designed physicochemical properties and surface modifications, the pharmacokinetics and pharmacodynamics can be distinctly improved (2). Typical applications of nanoparticles include drug solubilization, crossing of biological barriers, controlled release, passive and active targeting, vaccination or immune modulation, and gene therapy (3). Such nanocarriers are often made of synthetic biodegradable polymers with a favorable toxicological profile. One of the best established polymers for biomedical applications is poly(lactic-co-glycolic acid) (PLGA) (3,4). Due to the biodegradability and biocompatibility of PLGA and its hydrolysis products, several PLGA-containing drug products are approved by the FDA.

While the encapsulation of hydrophobic molecules into polymeric nanoparticles usually can be achieved with good efficiency by nanoprecipitation—a method initially developed by Fessi *et al.* (5)—more complex methods are needed to formulate hydrophilic entities like proteins. One of the most widely used approaches is the double emulsion method (6): an aqueous solution of the hydrophilic drug is emulsified into a non- or partially miscible solvent containing the polymer. To this emulsion, a second aqueous phase containing a stabilizer is added and the mixture further homogenized. After solvent removal the polymer precipitates, entrapping the drug within the newly formed particles. Currently employed devices for the critical homogenization step include high shear mixers, probe sonicators, high pressure homogenizers and microfluidic systems, although numerous issues can render them unsuitable for a range of applications. Direct sample contact may lead to cross-contamination or a reduced sample throughput at best, due to the necessity of thorough equipment cleaning. A serious temperature gradient throughout the sample may affect protein stability, while product contamination due to open setups and metal abrasion interferes with parenteral dosing and immunological readouts. Maybe the most important issue of established homogenization techniques is the missing scalability to adapt the produced amount from the bench to the clinic. While there was already some work done on the scale up of lab scale processes (7–10), these mostly include the use of bigger reactors, different geometries, or even different equipment. Furthermore, information on the scale up of actual pharmaceutical nanoparticle production processes for clinical products is very scarce (11). A single piece of equipment that covers early stage formulation screening all the way to proof-of-concept might considerably advance the somewhat obstructed translation of nanomedicines to patients (12).

For this reason, we investigated focused ultrasound as a scalable and contact-free homogenization technique to produce polymeric nanoparticles by the double emulsion method. In contrast to classical probe sonicators which are directly submerged in the sample, focused ultrasound uses a concave transducer which bundles the acoustic waves in a focal point within a closed vessel. The induced cavitation leads, similar to probe sonication, to an energy input and thus to a size reduction of emulsion droplets and subsequently nanoparticles. However, acoustic focusing avoids the formation of complex interference patterns and associated pressure hot spots throughout the sample and cooling bath, as is common with unfocused probe or bath sonication. A slight but constant variation of the emitted acoustic wavelength shifts the focal point for better sample mixing.

This leads to a better energy distribution and process reproducibility. Furthermore, the heat generated by the vibration of the transducer is not absorbed by the sample but rather by a surrounding water bath. In consequence, all these factors help to avoid thermal input into the system and degradation of the drugs. Due to disposable vials and flow cells, the same equipment may be used to process sample volumes from 100 μL to 20 mL in batch mode and from 50 mL up to several liters in continuous mode.

In the present study we show the feasibility to use focused ultrasound to encapsulate the widely used model antigen ovalbumin in PLGA nanoparticles in a production scale from 1 mg to 2.5 g polymer mass. The influence of process parameters on nanoparticle size and yield, drug load, and process scalability was investigated, and a nanoparticle purification protocol suitable for large suspension volumes was successfully established.

MATERIALS AND METHODS

Materials

Poly(lactic-co-glycolic acid) (PLGA, Resomer® RG 503 H; LA:GA = 50:50, 24–38 kD, free carboxylic end group) was purchased from Evonik Industries (Essen, Germany). Ovalbumin grade V was obtained from Sigma Aldrich (St. Louis, USA). Poloxamer 407 (P-407) was kindly provided by BASF (Ludwigshafen, Germany; Lutrol® F127). All other chemicals were obtained from Merck KGaA (Darmstadt, Germany) in analytical or HPLC grade.

Nanoparticle Preparation

All solutions were freshly prepared and filtered through 0.2 μm PTFE (polytetrafluoroethylene; for organic solvents) or PES (polyethersulfone; for aqueous solutions) membrane filters before use. A modified double emulsion solvent evaporation method was used to prepare Ovalbumin-loaded PLGA nanoparticles (13). In brief, 12 mg/mL PLGA was dissolved in ethyl acetate (EtOAc), added to an aqueous solution of 3.75 mg/mL ovalbumin, and the mixture was homogenized using focused ultrasound (Covaris S220x, LGC-KBioscience, Teddington, UK) as described in the section below. To this

primary W/O emulsion, an aqueous solution of 5 mg/mL P-407 was added and the mixture emulsified again by focused ultrasound. EtOAc was removed from this secondary emulsion overnight under magnetic stirring in a fume hood resulting in formation of PLGA nanoparticles. Water lost during evaporation was replaced, yielding an aqueous suspension with nominal concentrations of 0.3 mg/mL ovalbumin, 6 mg/mL PLGA, and 5 mg/mL P-407. The resulting suspension was centrifuged for 15 min at 1,000×*g* to remove larger aggregates. 1 mL aliquots of the supernatant were centrifuged for 10 min at 21,000×*g*, and the nanoparticle pellet was washed and redispersed in particle-free, deionized water (Milli-Q, Merck Millipore, Billerica, USA).

Table I shows the volumes of PLGA, ovalbumin, and P-407 solutions used to prepare PLGA nanoparticles in different batch sizes.

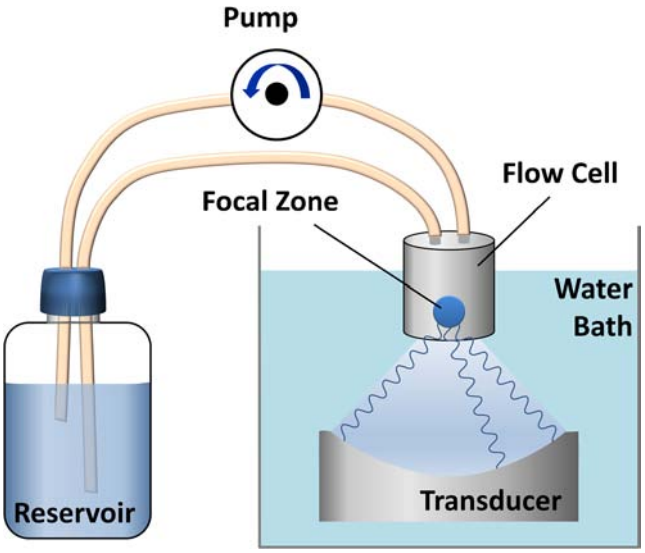

Fig. 1 Schematic of focused ultrasound with flow cell. In the case of batch processing the flow cell would be simply substituted with a closed glass vial.

Focused Ultrasound Treatment

The Covaris instrument consists of a concave transducer submerged in a water bath. Acoustic waves are conveyed through the water (degassed and conditioned at 7°C±2°C) to the focal point in the submerged sample vessel. Either closed glass tubes or a sonication flow cell were used. The flow cell is a 22 mL steel cylinder with two tubing connectors and a thin sheet of polyimide (Kapton®) facing the transducer. In our setup, the sample was continuously circulated from a bulk vessel to the flow cell and back by a peristaltic pump (Fig. 1). Samples were taken from the bulk vessel at predetermined time points during the second emulsification step. Device settings and derived parameters are summarized in Table II.

Nanoparticle Characterization

Particle sizes and size distributions were determined by dynamic light scattering (DLS) using a Zetasizer Nano ZS (Malvern Instruments, Worcestershire, UK) equipped with a helium neon laser (λ=633 nm). Samples were diluted 1:100 with Milli-Q water, measured three times at 25.0±0.1°C using backscatter mode (173°), and data was analyzed using cumulants fit.

The presence of multiple particle populations and the particle size distribution before any washing steps were determined by static light scattering using a Horiba LA-950 V2 (Retsch Technology, Haan, Germany). Particle suspensions were added to a MiniFlow circulating system to achieve a transmission between 80% and 90% at λ=405 nm. Analysis was performed according to Mie scattering theory with a refractive index of PLGA of 1.44 – 0.01i (14).

To determine the process yield and ovalbumin loading, 1 mL particle suspension was dried in a rotational vacuum concentrator (RVC 2–33 IR, Martin Christ, Osterode, Germany). The dry nanoparticles were weighed, dissolved in 1 M NaOH, neutralized with 1 M HCl and the protein content measured with a BCA protein assay kit according to the manufacturer's instructions (Merck Millipore, Billerica, USA). The total protein recovery of this method was previously validated by CHN elemental analysis (data not shown). Process yield and ovalbumin loading were calculated using the following equations:

$$\textit{Process Yield} = \frac{\textit{Nanoparticle mass}}{\textit{initial mass of PLGA and Ovalbumin}} \times 100\% \quad (1)$$

$$\textit{Ovalbumin loading} = \frac{\textit{Ovalbumin mass}}{\textit{Nanoparticle mass}} \times 100\% \quad (2)$$

Influence of Focused Ultrasound on Ovalbumin Stability

An ovalbumin solution similar in concentration and volume to a typical experiment (0.38 mg/mL in 100 mL) was circulated

Table I Composition of Emulsions Used to Prepare PLGA Nanoparticles in Different Batch Volumes. The Used Sonication Vessels were 300 μL and 16 mL Glass Vials, and a 22 mL Stainless Steel Flow Cell

Identifier	Vial 0.3 mL (μL)	Vial 8 mL (mL)	Flow Cell 95 mL (mL)	Flow Cell 665 mL (mL)
Ovalbumin in water	15.2	0.4	4.8	33.6
PLGA in EtOAc	95	2.5	30	210
P-407 in water	190	5.0	60	420
Total filling volume	300.2	7.9	94.8	663.6

Table II Settings and Derived Parameters for the Covaris Focused Ultrasound Device

Abb.	Parameter	Description
DF	Duty Factor	The percentage of time the transducer emits acoustic energy.
CpB	Cycles per Burst	The number of acoustic oscillations (cycles) during an "on" period of the transducer (burst).
PIP	Peak Incident Power	Sonic power (in W) applied to the sample during an "on" period.
AIP	Average Incident Power	Can be approximated as *AIP*≈*DF x PIP*. The calculated *AIP* may differ from measured AIP due to constructive or destructive interference of generated and reflected sonic waves.
E	Total Incident Energy	The product of *AIP* and treatment time *t*.
E/V	Incident energy per unit volume	The quotient of *E* and batch volume *V*.

through a sonication flow cell and treated with maximum intensity (250 W average incident power) up to 40 min. Samples were taken at predetermined time points and ovalbumin integrity determined by size exclusion high performance liquid chromatography. A TSKgel® SuperSW2000 column (Tosoh Bioscience, Stuttgart, Germany) was used at 25°C with an eluent containing 0.05 M sodium phosphate buffer pH 7.0 and 0.15 M sodium perchlorate. The flow rate was set to 0.45 mL/min and the UV absorption was measured at 214 nm. To calculate the ratio of ovalbumin monomer to aggregates and fragments, all relevant peaks were integrated and divided by the total integrated area before treatment.

Crossflow Filtration Method Development

A purification protocol was developed for MicroKros® hollow fiber crossflow filtration modules (modified polyethersulfone (mPES) membrane, 500 kD MWCO, 20 cm^2 surface area; Spectrum Laboratories, Rancho Dominguez, USA). A diafiltration setup was used for purification, *i.e.*, the volume of the retentate was kept constant by continuously replacing the filtrated volume with fresh medium. The replaced medium is measured in diafiltration volumes (DV), where one DV is defined as the volume of the process solution at the start of the diafiltration. If the membrane transmission of a compound is known, the concentration reduction of the compound in the retentate *CR* can be predicted as follows:

$$CR = 1 - e^{-DV \times \tau} \tag{3}$$

where τ is the transmission coefficient of the solute—with $\tau = 1$ meaning free transmission, and $\tau = 0$ meaning no transmission (15). Equation (3) is only valid if τ is independent from solute concentration and the transmembrane pressure is kept constant. Consequently, the transmission coefficient can be calculated by measuring *CR* and solving Eq. (3) for τ:

$$\tau = -\frac{ln\,(1-CR)}{DV} \tag{4}$$

To determine the transmission coefficient of P-407, 50 mL of a 5 mg/mL P-407 solution were circulated from a bulk vessel to the diafiltration module and back. The filtrated volume was continuously replaced by Milli-Q water. Samples were taken from the permeate and the concentration of P-407 was determined by gel permeation chromatography (GPC) using a Tosoh TSKgel® G3000H_{HR} column at 60°C, dimethylformamide as eluent at 1.2 mL/min, and a refractive index detector. The concentration reduction of P-407 in the retentate *CR* was calculated using the equation:

$$CR = \frac{c_P \times V_P}{m_0} \times 100\% \tag{5}$$

where m_0 is the total mass of P-407 at the start of the diafiltration, c_P is the concentration of P-407 in the permeate and V_P is the volume of the permeate. The transmission coefficient subsequently can be calculated for the respective number of diafiltration volumes by Eq. (4). At the end of each experiment, the residual concentration of P-407 was directly determined from the retentate.

Nanoparticle Suspension Purification

Ten milliliters of a freshly prepared PLGA nanoparticle suspension was diluted to 20 mL with Milli-Q water and circulated at 40 mL/min through a pre-washed MicroKros® module. The permeate was replaced with Milli-Q water at the same rate to perform a diafiltration. At the end of the diafiltration the suspension was concentrated to 7 mL, the filtration module completely emptied, rinsed with 2 mL of Milli-Q water and the combined retentate diluted to 10 mL.

RESULTS AND DISCUSSION

To our knowledge, this is the first study on the preparation of polymeric nanoparticles using focused ultrasound and the double emulsion method. Therefore, optimal treatment

parameters were established experimentally by investigating the influence of the sonication intensity and time on particle size, ovalbumin loading capacity and nanoparticle yield. The study was started with a batch size of 8 mL in disposable glass vials to obtain sufficient material for analysis while keeping the material need at minimum. We could quickly discard settings with low duty factor (DF) or peak incident power (PIP) as a certain minimum sonication intensity is necessary to induce cavitation and therefore to reduce droplet size. There was no pronounced difference in particle size when lowering DF and raising PIP accordingly to keep the average incident power (AIP; equals roughly the product of DF and PIP) constant. Because of the good reproducibility the DF was kept constant at DF 50% for the following experiments. A preliminary stabilizer screening was conducted, including polyvinyl alcohol, poloxamer 188, poloxamer 407, dimethyldidodecylammonium bromide, sodium deoxycholate, and Tween 80 at concentrations between 0.1 and 2% (supplementary material). Poloxamer 407 was chosen due to its ability to form nanoparticles with small size and narrow size distribution. Furthermore, P-407 could adequately stabilize both the emulsion as well as the subsequently formed nanoparticles at a relatively low concentration (Figures S1 and S2).

Nanoparticle Size

Figure 2 shows the correlation between ultrasound treatment time and the resulting mean particle size after collection of the nanoparticle population. At all investigated time points, the nanoparticle size distribution was narrow (polydispersity index <0.2). A mean particle size of 200 nm can be achieved with very short processing times. The size decrease is faster at the beginning of the ultrasound treatment, and the mean nanoparticle size eventually approaches a minimum between 105 and 110 nm. A similar trend was observed previously (16,17), although Feczkó *et al.* reported a minimum size of 140 nm using a similar PLGA concentration, but different solvent and stabilizer. As would be expected, particle size is generally decreased with ongoing treatment, and the size reduction is faster when increasing the average incident power (AIP) from 50 W to 100 W (Fig. 2a). As the particle size is mainly determined by the size of the emulsion droplets, which in turn depends on the energy used for homogenization, it is not surprising that the particle size curves of both treatments become nearly identical when normalizing on total incident energy as the product of AIP and treatment time (Fig. 2b). This interdependence between ultrasound intensity and treatment time makes the process very predictable and therefore provides an advantage during method development.

In this setup, the particle diameter D can be calculated from the incident energy E as follows:

$$D(E) = \frac{a}{b+E} + c \tag{6}$$

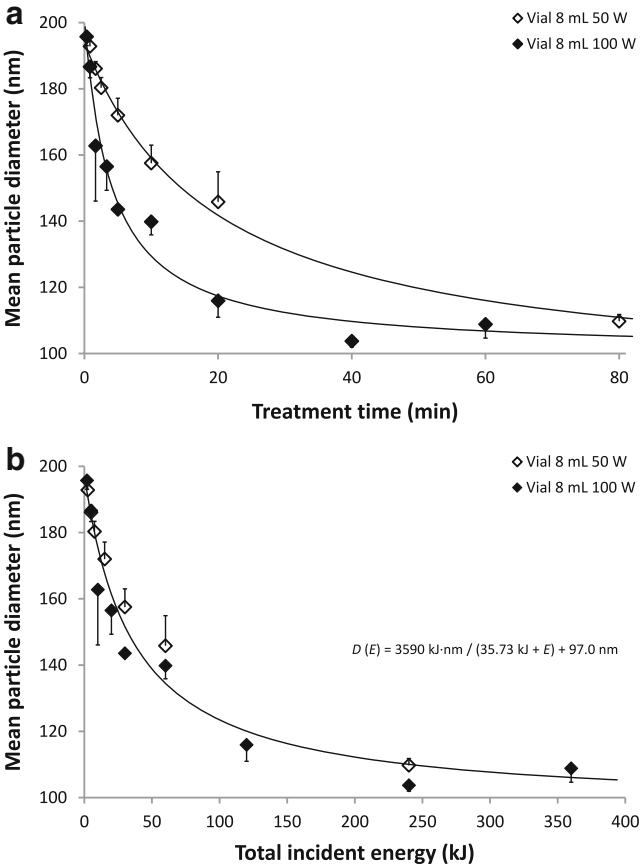

Fig. 2 Mean particle size of formulations manufactured with different Average Incident Power as a function of (**a**) sonication time (starting from several seconds) and (**b**) total incident energy. The size of three independent batches per time point was determined by DLS and the standard deviation depicted as error bars.

where a defines the initial steepness of the curve and as such probably includes factors like temperature, PLGA concentration, emulsion viscosity, sample volume, and the ratio water/organic phase.

The parameter b defines the pole of the function at $E=-b$. The fact that $b>0$ means that a very low amount of nanoparticles may be found even with no second emulsion at all. Due to the removal of microparticles and larger aggregates during the first centrifugation step at $1.000\times g$, this very low amount of nanoparticles is detectable by dynamic light scattering, and a mean diameter for this nanoparticle population can be measured. This phenomenon has its origin most probably in the physical forces upon contact of the first emulsion with the P-407 solution, as EtOAc is partially miscible with water and both phases will saturate each other.

The parameter c defines the asymptote of the function and corresponds to the minimum emulsion droplet size after droplet breakup and recoalescence during ultrasound-induced cavitation. Factors influencing c most probably include surface tension, type and concentration of stabilizer, PLGA concentration, and viscosity.

Nanoparticle Yield

While the nanoparticle size is continuously decreased with progressing treatment time, the nanoparticle yield rises for both the 50 W and 100 W treatments to optimal values of 47–63% at 10–30 kJ total incident energy, but declines when further prolonging treatment (Fig. 3). As expected, a higher intensity leads to a faster increase in yield, and when normalizing again on total incident energy the nanoparticle yield from both treatments follow the same trend, again indicating a predictable process. Interestingly, this biphasic relationship of nanoparticle yield Y and total incident energy E can be described by a simple function (Fig. 3, solid line):

$$\boldsymbol{Y(E)} = \boldsymbol{aE^{-1}} + \boldsymbol{bE} + \boldsymbol{c} \quad (\boldsymbol{a}, \boldsymbol{b} < 0) \tag{7}$$

As a centrifuge step during the manufacturing process separates the nanoparticles from larger particles, it is safe to assume that the major reason for increasing yield in the beginning of the process is the size reduction of bigger emulsion droplets to submicron size. To elucidate this, static light scattering measurements of the particle suspensions were performed before any centrifuge separation during the positive slope of the curve ($E<$ 27 kJ). After 20 s at 100 W AIP (or 2 kJ), two distinct particle populations exist in the submicron and micron size range, respectively (Fig. 4, dotted line). When increasing treatment time, the microparticle population diminishes in favor of the submicron population, and eventually after 20 kJ (Fig. 4, solid line) only the submicron population remains. The transition from one population to the other is not continuous, as the mode of the particle size of the microparticle population does not change and both nanoparticle and microparticle size peaks remain clearly separated. This is in accordance with the mechanism of emulsion droplet size reduction by cavitation which is deformation and sudden break-up of droplets (18).

Consequently, the total conversion of micron to submicron droplets (and therefore the maximum yield gain due to this process) coincides with the observed peak values for the nanoparticle yield between 10 and 30 kJ (Fig. 3). We therefore conclude that due to the steep rise and eventual asymptotic behavior, the term aE^{-1} ($a<0$) from Eq. (7) is reasonable for a mathematical description of the yield gain resulting from droplet size reduction.

Yield diminishing influences are accounted for by the second term from Eq. (7) bE ($b<0$). Especially at incident energies below 100–200 kJ the yield reduction coincides with a particle size reduction (Fig. 5). There are several explanations for this correlation. First, if the stabilizer concentration is just enough to stabilize an emulsion, the increased total surface area as a result of emulsion droplet size reduction may lead to a decrease of local stabilizer concentration at the interface and consequently to droplet re-coalescence and emulsion instability after treatment. Second, if the surface of subsequently formed particles is not saturated with stabilizer, aggregation might occur during centrifuge purification. Third, smaller particles are more likely lost during centrifugation as the RCF was kept constant. Consequently, when substituting

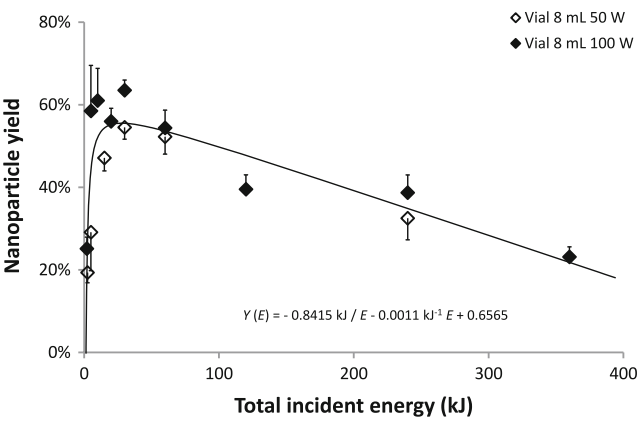

Fig. 3 Nanoparticle production yield as a function of total incident energy. Three independent batches per time point were washed, dried, weighed, and the yield calculated by Eq. (1). *Error bars* represent the standard deviation.

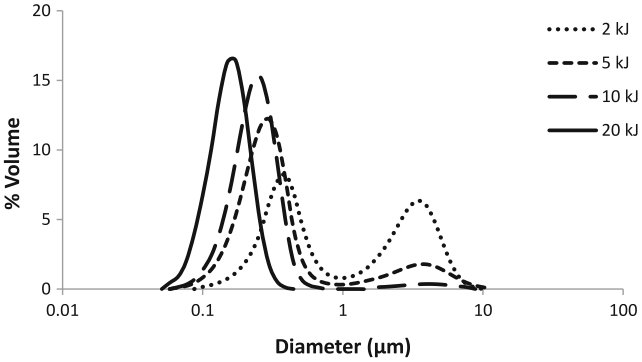

Fig. 4 Particle size distribution of formulations prepared with increasing treatment times and 100 W AIP. Measurements were made by static light scattering before any washing steps.

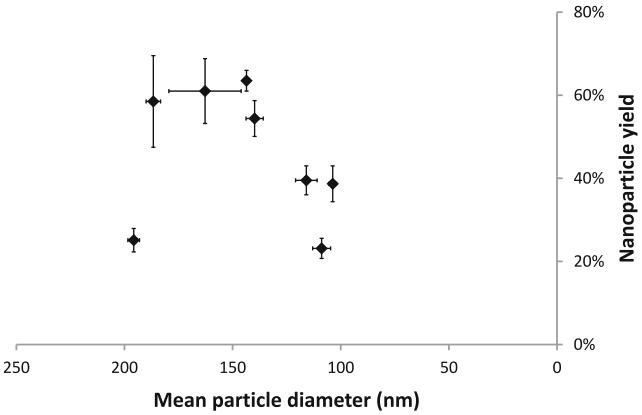

Fig. 5 Correlation between mean nanoparticle size and nanoparticle yield. Eight milliliters emulsion was treated in a glass vessel at 100 W AIP. The horizontal axis was mirrored to clarify the chronological progression from larger to smaller particles during the course of the process. Centrifuge purification is most likely the reason for reduced yield when producing smaller nanoparticles.

centrifuge purification for crossflow filtration, thus eliminating two of the possible reasons, we could significantly increase the yield (see section "Crossflow Filtration").

While the particle size decreases only slightly further at incident energies above 100 kJ, there is still a noticeable drop in nanoparticle yield (Figs. 2b and 3). Considering the small batch volume of 8 mL and the very long treatment time—which is well beyond reasonable process times for production—degradation might occur due to mechanical stress and the generation of free hydroxyl radicals in the process of cavitation. A cleavage of PLGA to water-soluble oligomers and monomers would reduce the mass of precipitable polymer, while a loss of stabilizer could lead to coalescence and aggregation as described above, both decreasing nanoparticle yield. The solvodynamic shear generated by the formation, oscillation and collapse of cavitation bubbles leads to a tension along the elongated polymer backbone and subsequent chain scission (19). Considering the γ-irradiation-induced radical decomposition of PLGA and polyethers like P-407 (20,21), cavitation induced free radicals might lead to a similar autoxidative decomposition pathway: C-H bond cleavage and peroxide formation in the presence of hydroxyl radicals and oxygen, random polymer chain cleavage, and eventually short chain acid formation (21,22).

Indeed, PLGA in dichloromethane was found to experience molecular weight loss when sonicated even at relatively low intensities with relatively short processing times (23). Reich found a significant molecular weight reduction when treating a 6 mL sample at 40 W for 30 s (=0.2 kJ/mL) with a submerged probe sonicator. While we did not systematically monitor the stability of PLGA and P-407 following sonication in this study, no degradation of either polymer could be detected in samples manufactured with an AIP of 50 W and 0.6 kJ/mL energy per unit volume (gel permeation chromatography data not shown). The superior polymer stability in our study may be explained by the controlled and contact-free nature of a focused ultrasound treatment as opposed to probe sonication; the latter suffering from unpredictable interference patterns and energy hotspots across the sample due to the unfocused distribution and reflection of sonic waves. Another factor might be the stabilizer P-407 used in our study, a tri-block copolymer of poly(oxyethylene) (POE) and poly(oxypropylene) (POP) in the form of POE_a-POP_b-POE_a with a = 101 and b = 56. POE was found by Rokita and Ulański to be an effective radical scavenger by investigating competition kinetics in a sonochemical reactor (24). Furthermore, they found that less hydrophobic polymers like POE are enriched at the gas/water interface of the cavitation bubbles up to a factor of 100 compared with the rest of the solution, while more hydrophobic polymers like poly(methyl methacrylate) are evenly distributed (24). Thus, by saturating the interface, the stabilizer might displace other molecules of interest from the zone of greatest stress and therefore additionally protects them from mechanical forces and free radicals.

Only at considerably higher incident energy ($E > 100$ kJ, equal to 12 kJ/mL for 8 mL sample), a decline of nanoparticle yield occurs which is probably related to polymer degradation. The needed energy is 60 times higher than the degradation threshold of PLGA reported by Reich (23). Based on these findings, a systematic assessment of the polymers' integrity depending on the used energy source, incident power and energy per unit volume is necessary for a rational manufacturing process design.

The linear constituent bE from Eq. (7) likely is too simplified to describe all underlying mechanisms of yield decline. However, degradation is only expected when overprocessing a sample, and the manipulation of both particle size and nanoparticle yield is effectively possible before reaching critical levels of incident energy. Therefore we conclude that the process preserves the structure of PLGA and P-407, and that the proposed equation is both mathematically reasonable and adequate for yield optimization.

Ovalbumin Loading

Ovalbumin was used as model protein due to its common usage in early vaccination studies with mice. The ovalbumin loading is at acceptable levels even after short processing times and seems to be higher at lower average incident power. During 50 W treatment the loading reaches a maximum of 3.6 ± 0.1% protein per particle weight at 150 s (equaling 7.5 kJ), while a 100 W treatment peaks at 3.2 ± 0.2% at 200 s (20 kJ) (Table III). This conforms to published work on the encapsulation of ovalbumin in PLGA using probe sonication with reported values from 1.2 to 5.4% (25–27). As we did not optimize the used concentrations of ovalbumin and PLGA

Table III Total Incident Energy (TIE) Necessary to Achieve Either Maximum Ovalbumin Loading or Ovalbumin Encapsulation Efficiency (EE) for Different Average Incident Power (AIP). EE is Calculated from Loading and Nanoparticle (NP) Yield

	TIE (kJ)	Energy per unit volume (kJ/mL)	Ova Loading (%)	NP Yield (%)	Ova EE (%)
AIP 50 W, max. load	7.5	0.9	3.6 ± 0.1	29.5 ± 3.1	22.4 ± 3.3
AIP 50 W, max. EE	30	3.8	3.3 ± 0.2	54.5 ± 4.2	38.2 ± 5.7
AIP 100 W, max. load and EE	20	2.5	3.2 ± 0.2	56.0 ± 3.2	38.1 ± 4.9
Literature (25–28)[a]	*n.a.*	0.1 − 1	1.2 − 5.4	*not reported*	15 − 34

[a] Comparison with probe sonication. Energy per unit volume was estimated as all suitable references lack information regarding one or more of the following: total volume, power source, applied power, pulsing, and ultrasound horn

during emulsification, the ovalbumin loading achievable by focused ultrasound may be higher than reported in this study. Especially when using costly proteins, the encapsulation efficiency (EE; the fraction of ovalbumin that is actually encapsulated in the nanoparticles) is another important factor. It can be calculated from the ovalbumin loading, the nanoparticle yield and the total amount of employed ovalbumin. For the above mentioned loading maxima the EE is 22 and 38% for the 50 W and 100 W treatments, respectively (Table III). This again conforms to published work with reported EE from 15 to 34% (26–28).

Similar to yield, when drastically increasing the incident energy to values above 100 kJ the loading seems to decrease again for the 50 W treatment (2.0% at 240 kJ). A similar trend was observed by Feczkó *et al.* who proposed a greater chance of drug escape from the inner aqueous droplets (which would get encapsulated) to the outer water phase for longer and higher intensity emulsification treatments (29). Interestingly, the loading increases to 6.6% when applying excessive incident energy (360 kJ at a power of 100 W AIP). As the protein visibly aggregates under these harsh conditions, this finding might have been caused by a changed affinity of ovalbumin oligomers to the polymer matrix, the formation of protein aggregates similar in size to the PLGA nanoparticles, or the formation of protein-polymer conjugates. The exact cause was not further investigated as relevant processing energies to achieve acceptable particle size, yield and loading are equal or below 30 kJ and thus more than ten times smaller.

Influence of Batch Volume

To assess the potential for discovery formulation screening with very limited amounts of drug substance, the method was adjusted from 8 mL to fit 300 µL glass sonication vials. This reduced the amount of PLGA necessary for one sample run from 30 mg to 1.1 mg. Although the maximum sonication intensity is limited for the smaller vessels, comparable energy per unit volume can be achieved. When normalizing the total energy intake on batch volume, the particle sizes for the 300 µL batches fit nicely into the curve extrapolated from the 8 mL batches (Fig. 6a). This indicates a good scalability between the two batch sizes and that particle sizes can be predicted by applying simple mathematics.

By using a stainless steel sonication flow cell, batch volumes of up to several liters can be processed with a single unit. As this would equal tens of grams of PLGA nanoparticles, the proposed method would also be suitable for the supply of larger pre-clinical studies. As the process is continuous, contact-free, and all parts with product contact are either sterile consumables or autoclavable, it may possibly be used for the supply of clinical trials. We therefore investigated the upscale potential by producing PLGA nanoparticles in batch sizes of

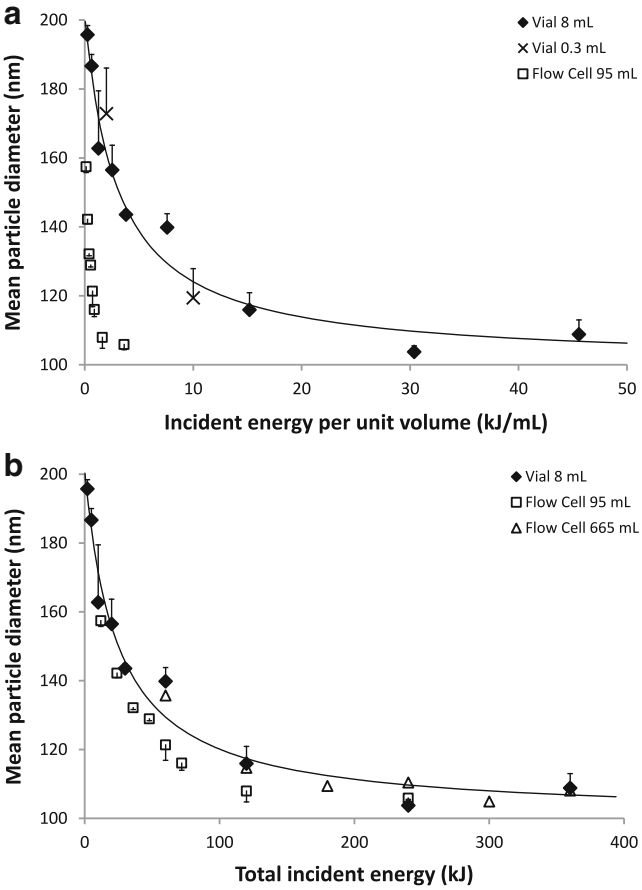

Fig. 6 Mean particle size of formulations with different batch volumes manufactured in different sonication vessels as a function of (**a**) energy density and (**b**) total incident energy. The average incident power was 100 W for the 8 mL and 95 mL batches, and 10 W for the 0.3 mL batch. *Symbols* represent mean ± standard deviation, $n = 3$ for 0.3 mL, 8 mL and 95 mL, $n = 1$ for 665 mL. The *solid line* is a fit for the 8 mL batch according to Eq. (6).

95 mL and 665 mL (360 mg and 2520 mg PLGA, respectively).

Particle sizes are reduced much more efficiently at same energy per volume levels in the flow cell than in the glass vessels (Fig. 6a). This may be due to a better acoustic transmissibility of the plain polyimide sheet at the bottom of the flow cell, while the curved bottom of the glass vials result in greater sonic wave reflection. In fact, when processing a batch volume of 665 mL the same particle size can be achieved as for the 8 mL batch in a glass vessel by using just the same amount of sonic energy (Fig. 6b).

While the flow cell is more effective regarding particle size reduction at a given energy level, the nanoparticle yield is inferior to the glass vessel application (maximum of 23.9 ± 5.7% at 2.5 kJ/mL *vs.* 63.5 ± 2.5% at 3.8 kJ/mL) (Fig. 7). Possible explanations are surface adsorption in the pump tubing, and incomplete mixing in the bulk vessel. In the resulting "dead volumes" droplets are less likely to be conveyed to the flow cell and may retain above-micron sizes (meaning lower nanoparticle yield), while the rest of the fluid is

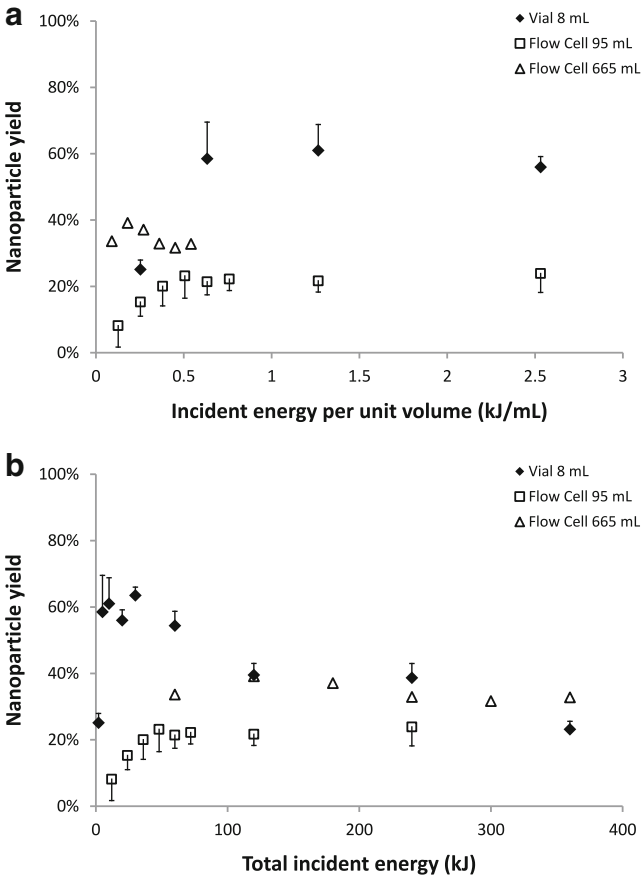

Fig. 7 Nanoparticle yield of formulations using either a glass vial or a flow cell as a function of (**a**) incident energy per batch volume and (**b**) total incident energy. The average incident power was 100 W for all batches. *Symbols* represent mean ± standard deviation, $n = 3$ for 0.3 mL, 8 mL and 95 mL, $n = 1$ for 665 mL.

disproportionately more sonicated (meaning smaller nanoparticles). Consequently, as fluid dynamics were easier to control in a larger scale, the 665 mL batch with a yield of 39.2% was superior to the 95 mL batch, but still not as efficient as the 8 mL process. This difference can be explained by the smaller particle size of flow cell *versus* glass vial preparations at lower energy levels, as smaller particles are lost to a greater extent during centrifuge washing (see section "Crossflow Filtration").

Similar to the nanoparticle yield, the ovalbumin loading achieved during the 95 mL process (0.5–1.0% for 0.1–2.5 kJ/mL) was inferior to the 8 mL process (2.0–3.6% for 0.3–7.6 kJ/mL). When further increasing the batch volume to 665 mL, a comparable loading is achievable by the flow cell process with lower incident energy per unit volume (1.6–2.5% for 0.1–0.6 kJ/mL). This indicates that a certain minimum volume is necessary for a representative flow cell treatment.

Ovalbumin Stability

Figure 8 shows the influence of focused ultrasound on the structure and stability of ovalbumin processed in a flow cell

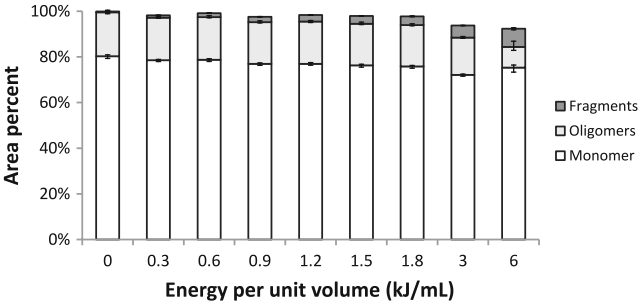

Fig. 8 Stability of ovalbumin during focused ultrasound processing of a solution in a flow cell (AIP 250 W). Protein structure was determined by size exclusion chromatography and quantified by integration of the acquired curve. All integrated peak areas for the respective species are reported as fraction of the total integrated area of an untreated sample (0 kJ/mL). *Bars* represent mean ± standard deviation of three independent treatments.

as obtained by size exclusion chromatography. Before the treatment, ovalbumin is present as 80.3% monomer, 19.2% soluble oligomers and very few to no fragments. At 0.6 kJ/mL (which is enough to reach an acceptable yield for flow cell processing) the monomer content is only slightly reduced from 80.3 to 78.8% of initial total integrated area, while the content of fragments rises from 0.4 to 1.7%. When drastically increasing the energy per unit volume to 6 kJ/mL, the monomer content is still relatively high at 75.3%, but a noticeable increase of fragments to 8.0%. The total integrated area of the size exclusion chromatogram decreases slightly above 0.9 kJ/mL. This is indicative of the formation of some insoluble degradation products. Overall the data shows that focused ultrasound itself has only a very slight effect on the structure of ovalbumin.

Optimization of the Washing Protocol

The nanoparticle mass loss can be partially contributed to the washing step. Higher energy treatments result in smaller particles, which in turn tend to form less dense pellets during

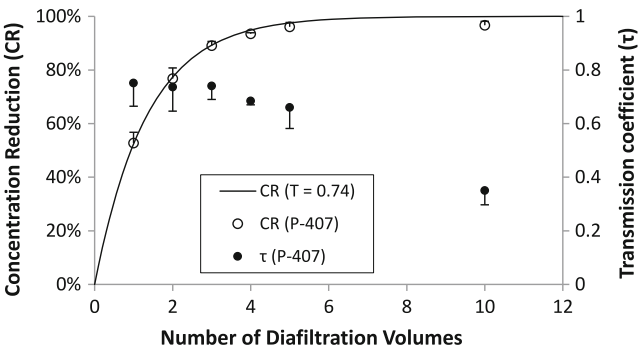

Fig. 9 Concentration reduction (*CR*) of poloxamer 407 in the retentate during diafiltration. The *open spheres* denote the *CR* of P-407 (determined from the permeate). *Solid spheres* denote the apparent membrane transmission of P-407 for the respective time point as calculated from *CR* using Eq. (4). The *line* shows the predicted *CR* for a compound with a concentration independent transmission of 0.74.

Table IV Crossflow Filtration of a Suspension of PLGA Nanoparticles Containing Ovalbumin. Mean and Standard Deviation are Calculated from Three Independent Filtration Experiments Using Different Filtration Modules

	Z-average diameter (nm)	Polydispersity index	Residual P-407	τ (P-407)	Residual ovalbumin
Before washing	122.1	0.098	100%	NA	100%
Crossflow filtration (DV = 5)	122.9 ± 1.6	0.106 ± 0.022	1.7 ± 0.2%	0.82	n.d.
Crossflow filtration (DV = 10)	122.4 ± 1.1	0.104 ± 0.015	<0.03% *	>0.80	<0.3% *

* Below LOQ

centrifugation and exhibit higher loss on washing. A simple solution would be to increase the relative centrifugal force (RCF). While this would reduce losses for smaller particles, preliminary trials suggested that bigger particles from lower energy treatments are more likely to deform or agglomerate at higher RCF, and may even form pellets that cannot be redispersed anymore. To optimize the nanoparticle yield while retaining the key formulation characteristics it would be necessary to establish individual washing protocols depending on the mean particle size of each preparation. Additionally, the feasible processing volume and scalability of centrifugation is limited.

To address these issues, crossflow filtration was established and compared to conventional centrifuge washing regarding purification efficiency, particle size distribution, ovalbumin loading capacity and overall production yield.

Crossflow Filtration

Membrane filtration is widely used for separation and purification purposes in biotechnology (30). In crossflow filtration, a solution or suspension is continuously pumped parallel to a membrane. The created transmembrane pressure forces the solvent and solutes smaller than the membrane's pores across the membrane, while the direction of the stream prevents membrane fouling. The used membranes are usually characterized by their molecular weight cut off (MWCO), indicating a 90% retention for globular macromolecules of that size.

In this study, the sub-micron particles are to be separated from excess ovalbumin (44.3 kDa) and P-407 (12.6 kDa on average). For optimal flux and upscale potential we chose a diafiltration module with a hydrophilic membrane formed to bundled hollow fibers. The fibers are made of modified polyethersulfone (mPES) with a MWCO of 500 kDa, equaling 20 nm according to the manufacturer. The nanoparticle suspension is circulated from a bulk vessel through the interior of the membrane fibers and back. Small molecules like solvents and salts readily cross the membrane to the exterior encasing where they are collected and flushed out. After 7 diafiltration volumes, the concentration of such molecules in the retentate is usually reduced below 0.1% of the initial value. More complex molecules like proteins and polymers may be filtrated if they are smaller than the membrane's pores, but exhibit a reduced transmission.

As this directly influences the efficiency of the purification, the transmission coefficient of P-407 in solution was determined from Eqs. (4) and (5) by repeatedly measuring the concentration of P-407 using GPC in the combined permeate during a diafiltration experiment (Fig. 9). During the first three diafiltration volumes, the transmission coefficient remains relatively unchanged at $\tau = 0.74 \pm 0.05$. With increasing diafiltration volumes (DV) the transmission seems to decrease. At the end of the experiment (after 10 DV), the amount of P-407 found in the permeate was 96.7%, and the transmission was calculated as $\tau = 0.35 \pm 0.05$. However, direct sampling from the retentate revealed that less than 0.1% P-407 (below limit of quantification) actually remained in the retentate, resulting in a transmission of at least 0.70 after 10 DV. Accordingly, the initially observed decline of membrane transmission is not an effect of concentration dependency but rather due to adsorption of P-407 to the tubing and the membrane.

To validate the findings in the presence of nanoparticles, a second diafiltration study was conducted with a freshly prepared nanoparticle suspension (6 mg/mL PLGA) containing ovalbumin. Particle sizes were measured by DLS before and after purification. The concentration of P-407 and ovalbumin was determined directly from the retentate by GPC and BCA assay, respectively. It was found that the particles remained stable during purification with no change in mean particle

Table V Influence of Washing Protocols on Formulation Parameters. Although the Variance Could not be Calculated Due to Sample Pooling ($n = 3$), the Polydispersity Index Is Sufficiently Low to Discern Safely Between the Two Washing Protocols

	Z-average diameter (nm)	Polydispersity index	Ovalbumin loading capacity (%)	Nanoparticle yield (%)
Before washing	172.7	0.084	n.a.	n.a.
Centrifuge washing	190.0	0.134	2.4	60.8
Crossflow filtration	168.9	0.124	2.2	73.8

diameter and size distribution (Table IV). This indicates that poloxamer 407 is effective as stabilizer during particle formation and purification, even after almost quantitative removal from the suspending liquid. This is in accordance with the hypothesis that the tri-block copolymer P-407 irreversibly adsorbs onto the surface of hydrophobic particles with its hydrophobic poly(oxypropylene) (POP) middle block, while the two poly(oxythylene) (POE) chains protrude into the surrounding medium (31,32). In contrast to our results, Quintanar-Guerrero *et al.* found that poly(lactic acid) nanoparticles stabilized with poloxamer 188 (P-188) agglomerate during diafiltration (33). Interestingly, the nanoparticles remained stable when they kept the concentration of P-188 constant during diafiltration, indicating a loose interaction between stabilizer and particle surface. The reason for the superior performance of P-407 is most likely the increased weight of the hydrophobic POP middle block (56 monomers as opposed to 27 in P-188). Indeed, field flow fractionation experiments showed that only the length of the POP chain influences the concentration of different poloxamers adsorbed to the surface of polystyrene nanoparticles of a given size, while the length of POE mainly influences the thickness of the adsorbed layer and the mobility of the protruding POE chains (34).

While a concentrated suspension of particles larger than the filter's pores would immediately block during conventional dead end filtration, no detrimental effect of PLGA nanoparticles on the removal of P-407 could be observed during crossflow filtration. The calculated transmission coefficient of P-407 ($\tau > 0.80$) was coherent with prior observations. It was concluded that a washing cycle of 9–10 DV is sufficient to reduce the amount of free stabilizer and protein to negligible levels (below 1 mg of free stabilizer per gram of nanoparticles).

In contrast to crossflow filtration, the purification of PLGA nanoparticles by centrifugation leads to a significant increase in mean particle size (Table V). While one would expect a somewhat lower ovalbumin load after 2 h of crossflow filtration and corresponding drug release, no difference could be observed to centrifuge purification. As expected, the overall nanoparticle yield could be further improved by the use of crossflow centrifugation. The described method is suitable for the described manufacturing process starting with batch volumes from 10 mL regardless of nanoparticle size. Only minor adjustments would be necessary to process different volumes. As hollow fiber modules are available with the same dimensions but with an increased number of fibers, a scale up to several liters seems to be reasonably simple.

CONCLUSION

A scalable and contact-free method to produce protein-loaded nanoparticles was successfully established based on a commercially available focused ultrasound transducer. Nanoparticles could be produced in batch sizes from 1 mg to 2500 mg using the same equipment. Similar nanoparticle characteristics could be achieved over the range of investigated batch sizes. The mean particle diameter could be controlled between 100 and 200 nm with a maximum yield of 74% and protein loading up to 3.6%. Lower yields for smaller particles and larger batch sizes could be mitigated by the use of diafiltration instead of centrifugation. The influence of device parameters and batch size on nanoparticle size and yield and could be described by simple mathematic relationships. This underlines the robustness and predictability of the process and therefor provides an advantage in method development and scale up. In contrast to already established methods, the proposed nanoparticle manufacturing process is a valuable tool for both screening purposes and manufacturing, and as such could advance the translation of nanomedicine to the clinic.

ACKNOWLEDGEMENTS AND DISCLOSURES

Parts of this work were funded by BMBF (German Federal Ministry of Education and Research) project PeTrA (ref. no. 13N11455). The authors are grateful for the technical assistance of Letícia Pires Rodrigues and Sebastian Franck.

REFERENCES

1. Etheridge ML, Campbell SA, Erdman AG, Haynes CL, Wolf SM, McCullough J. The big picture on nanomedicine: the state of investigational and approved nanomedicine products. Nanomed Nanotechnol Biol Med. 2013;9(1):1–14.
2. Davis ME, Chen Z, Shin DM. Nanoparticle therapeutics: an emerging treatment modality for cancer. Nat Rev Drug Discov. 2008;7(9):771–82.
3. Danhier F, Ansorena E, Silva JM, Coco R, Le Breton A, Préat V. PLGA-based nanoparticles: an overview of biomedical applications. J Control Release. 2012;161(2):505–22.
4. Jain AK, Das M, Swarnakar NK, Jain S. Engineered PLGA nanoparticles: an emerging delivery tool in cancer therapeutics. Crit Rev Ther Drug Carrier Syst. 2011;28(1):1–45.
5. Fessi H, Puisieux F, Devissaguet JP, Ammoury N, Benita S. Nanocapsule formation by interfacial polymer deposition following solvent displacement. Int J Pharm. 1989;55(1):R1–4.
6. Rao JP, Geckeler KE. Polymer nanoparticles: preparation techniques and size-control parameters. Prog Polym Sci. 2011;36(7):887–913.
7. Colombo AP, Briançon S, Lieto J, Fessi H. Project, design, and use of a pilot plant for nanocapsule production. Drug Dev Ind Pharm. 2001;27(10):1063–72.
8. Galindo-Rodríguez SA, Puel F, Briançon S, Allémann E, Doelker E, Fessi H. Comparative scale-up of three methods for producing ibuprofen-loaded nanoparticles. Eur J Pharm Sci. 2005;25(4–5):357–67.
9. Tewa-Tagne P, Briançon S, Fessi H. Preparation of redispersible dry nanocapsules by means of spray-drying: development and characterisation. Eur J Pharm Sci. 2007;30(2):124–35.
10. Rietscher R, Thum C, Lehr CM, Schneider M. Semi-automated nanoprecipitation-system-an option for operator independent,

scalable and size adjustable nanoparticle synthesis. Pharm Res [Internet]. 2014. doi:10.1007/s11095-014-1612-z.
11. Vauthier C, Bouchemal K. Methods for the preparation and manufacture of polymeric nanoparticles. Pharm Res. 2009;26(5):1025–58.
12. Lavik E, von Recum H. The role of nanomaterials in translational medicine. ACS Nano. 2011;5(5):3419–24.
13. Blanco MD, Alonso MJ. Development and characterization of protein-loaded poly(lactide-co-glycolide) nanospheres. Eur J Pharm Biopharm. 1997;43(3):287–94.
14. Schalper K. Herstellung hochdisperser Systeme mit kontinuierlichen Mikromischern [PhD thesis]. Berlin: Freie Universität Berlin; 2002.
15. Kovács Z, Fikar M, Czermak P. Mathematical modeling of diafiltration. Hung J Ind Chem. 2009;37(2):159–64.
16. Feczkó T, Tóth J, Dosa G, Gyenis J. Influence of process conditions on the mean size of PLGA nanoparticles. Chem Eng Process Process Intensif. 2011;50(8):846–53.
17. Bilati U, Allémann E, Doelker E. Sonication parameters for the preparation of biodegradable nanocapsulesof controlled size by the double emulsion method. Pharm Dev Technol. 2003;8(1):1–9.
18. Tadros T, Izquierdo P, Esquena J, Solans C. Formation and stability of nano-emulsions. Adv Colloid Interface Sci. 2004;108–109:303–18.
19. Caruso MM, Davis DA, Shen Q, Odom SA, Sottos NR, White SR, *et al.* Mechanically-induced chemical changes in polymeric materials. Chem Rev. 2009;109(11):5755–98.
20. Conti B, Dorati R, Colonna C, Genta I. Effects of ionizing radiation sterilization on microparticulate drug delivery systems based on poly-α-hydroxyacids: an overview. J Drug Deliv Sci Technol. 2009;19(2):99–112.
21. Kerwin BA. Polysorbates 20 and 80 used in the formulation of protein biotherapeutics: Structure and degradation pathways. J Pharm Sci. 2008;97(8):2924–35.
22. Donbrow M, Hamburger R, Azaz E, Pillersdorf A. Development of acidity in non-ionic surfactants: formic and acetic acid. Analyst. 1978;103(1225):400–2.
23. Reich G. Ultrasound-induced degradation of PLA and PLGA during microsphere processing: influence of formulation variables. Eur J Pharm Biopharm. 1998;45(2):165–71.
24. Rokita B, Ulański P. Studies on the spatial distribution of polymeric reagents in sonochemical reactions: application of competitive kinetics. Polimery. 2005;50(1):29–36.
25. Demento SL, Eisenbarth SC, Foellmer HG, Platt C, Caplan MJ, Mark Saltzman W, *et al.* Inflammasome-activating nanoparticles as modular systems for optimizing vaccine efficacy. Vaccine. 2009;27(23):3013–21.
26. Fievez V, Plapied L, des Rieux A, Pourcelle V, Freichels H, Wascotte V, *et al.* Targeting nanoparticles to M cells with non-peptidic ligands for oral vaccination. Eur J Pharm Biopharm. 2009;73(1):16–24.
27. Mittal A, Raber AS, Schaefer UF, Weissmann S, Ebensen T, Schulze K, *et al.* Non-invasive delivery of nanoparticles to hair follicles: a perspective for transcutaneous immunization. Vaccine. 2013;31(34):3442–51.
28. Slütter B, Bal S, Keijzer C, Mallants R, Hagenaars N, Que I, et al. Nasal vaccination with N-trimethyl chitosan and PLGA based nanoparticles: nanoparticle characteristics determine quality and strength of the antibody response in mice against the encapsulated antigen. Vaccine. 2010;28(38):6282–91.
29. Feczkó T, Tóth J, Dosa G, Gyenis J. Optimization of protein encapsulation in PLGA nanoparticles. Chem Eng Process Process Intensif. 2011;50(8):757–65.
30. van Reis R, Zydney A. Bioprocess membrane technology. J Membr Sci. 2007;297(1–2):16–50.
31. Scholes PD, Coombes AGA, Illum L, Davis SS, Watts JF, Ustariz C, *et al.* Detection and determination of surface levels of poloxamer and PVA surfactant on biodegradable nanospheres using SSIMS and XPS. J Control Release. 1999;59(3):261–78.
32. Blunk T, Hochstrasser DF, Sanchez JC, Müller BW, Müller RH. Colloidal carriers for intravenous drug targeting: Plasma protein adsorption patterns on surface-modified latex particles evaluated by two-dimensional polyacrylamide gel electrophoresis. Electrophoresis. 1993;14(1):1382–7.
33. Quintanar-Guerrero D, Ganem-Quintanar A, Allemann E, Fessi H, Doelker E. Influence of the stabilizer coating layer on the purification and freeze-drying of poly(D, L-lactic acid) nanoparticles prepared by an emulsion-diffusion technique. J Microencapsul. 1998;15(1):107–19.
34. Li J-T, Caldwell KD, Rapoport N. Surface properties of pluronic-coated polymeric colloids. Langmuir. 1994;10(12):4475–82.